Article:

Li, Z, Zhang, YG, Torres, M et al. (1 more author) (2023) Neogene burial of organic carbon in the global ocean. Nature, 613 (7942). pp. 90-95. ISSN 0028-0836

https://doi.org/10.1038/s41586-022-05413-6

Neogene burial of organic carbon in the global ocean

Ziye Li[1,2,3], Yi Ge Zhang[2*], Mark Torres[4] and Benjamin J. W. Mills[5]

[1]College of Marine Geosciences, Ocean University of China, Qingdao, 266100, China
[2]Department of Oceanography, Texas A&M University, College Station, TX 77843, USA
[3]MARUM-Center for Marine Environmental Sciences, University of Bremen, 28359 Bremen, Germany
[4]Department of Earth Science, Rice University, Houston, TX 77005, USA
[5]School of Earth and Environment, University of Leeds, Leeds, LS2 9JT, UK

*Corresponding Author.
Department of Oceanography, Texas A&M University, TX 77843, USA

yige.zhang@tamu.edu

Organic carbon buried in marine sediment serves as a net sink for atmospheric carbon dioxide and a source of oxygen[1, 2]. The rate of organic carbon burial through geologic history is conventionally established by using the mass balance between inorganic and organic carbon, each with distinct carbon isotopic values ($\delta^{13}C$)[3, 4]. This method is complicated by large uncertainties, however, and has not been tested with organic carbon accumulation data[5, 6]. Here we report a "bottom up" approach for calculating the rate of organic carbon burial that is independent from mass balance calculations. We use data from 81 globally distributed sites to establish the history of organic carbon burial during the Neogene (~23– 3 million years ago). Our results show larger spatiotemporal variability of organic carbon burial than previously estimated[7, 8, 9]. Globally, the burial rate is high towards the early Miocene and Pliocene and lowest during the mid-Miocene, with the latter period characterised by the lowest ratio of organic-to-carbonate burial rates. This is in contrast to earlier work that interpreted enriched carbonate ^{13}C values of the mid-Miocene as massive organic carbon burial (i.e. the Monterey Hypothesis)[10, 11]. Suppressed organic carbon burial during the warm mid-Miocene is probably related to temperature-dependent bacterial degradation of organic matter[12, 13], suggesting that the organic carbon cycle acted as positive feedback of past global warming, with implications for our future.

In the long-term carbon cycle, carbon dioxide is added to the surficial system through volcanic and metamorphic degassing and the weathering of sedimentary carbon, and is removed through the deposition of carbonates following chemical weathering of Ca-Mg silicate rocks and the burial of organic carbon (OC). The buried OC in marine sediment, on average only 0.1% of the primary production, is effectively isolated from the Earth's surficial system and therefore serves as a net sink for atmospheric CO_2, a source for O_2, and largely contributed to the occurrence of fossil fuels (Ref [1, 2]).

Traditionally, the fraction of carbon buried as organic carbon (f_{org}) is estimated through "top-down" isotopic mass balance approaches. The rationale is that there is a large carbon isotope fractionation associated with photosynthesis, which allows the carbon isotope signature of marine carbonates ($\delta^{13}C_{IC}$) to be used for calculating the fraction of organic vs. inorganic carbon in the total burial flux[3, 4, 6]. Assuming a steady state wherein the isotopic composition of carbon input to and output from the surficial system are balanced, then

$$C_{in} \times \delta^{13}C = C_{out} \times \delta^{13}C, \qquad \text{Equation 1}$$

$$\delta^{13}C_{in} = \delta^{13}C_{org} \times f_{org} + \delta^{13}C_{IC} \times (1 - f_{org}) \qquad \text{Equation 2}$$

It is often assumed that the average isotopic composition of carbon input ($\delta^{13}C_{in}$) is constant and approximately equal to mantle-sourced volcanic outgassing (-6‰ ± 1‰)[14]. Thus, the portion of carbon buried as organic matter (f_{org}) can be simply calculated if the $\delta^{13}C_{org}$ and $\delta^{13}C_{IC}$ are known. Positive $\delta^{13}C$ excursions of marine carbonates are commonly interpreted as enhanced organic carbon burial over carbonates. For example, during the Neogene period (ca. 23-3 million years ago, Ma), the heaviest $\delta^{13}C_{IC}$ occurred during the mid-Miocene, which coincides with the OC-rich shale deposits in California known as the "Monterey Formation". The famous "Monterey Hypothesis" argues that the $\delta^{13}C_{IC}$ maxima roughly 16-14 Ma represents globally enhanced OC burial and preservation, which led to subsequent CO_2 drawdown, global cooling, and expansion of ice sheets in East Antarctica during the Middle

Miocene Climate Transition (~14 Ma)[10, 11].

However, the assumption of a stable flux of carbon input with constant isotopic values has been challenged. For example, although the chemical weathering of silicate rocks has been extensively studied, changes of the weathering flux of organic-rich black shale, which is largely responsible for the long-term influx of ^{13}C-depleted CO_2 into the atmosphere, are largely unconstrained[15, 16]. Also, depending on the source of the carbon, volcanic and metamorphic CO_2 could vary significantly in its $\delta^{13}C$ values (-1 to -11 ‰)[17]. Lastly, authigenic carbonates formed as a consequence of anaerobic organic matter oxidation and characterized by relatively negative $\delta^{13}C$ values, would also complicate mass balance calculations[18, 19].

In this study, we establish the rate of global organic carbon burial over the Neogene period by utilizing measurements of total organic carbon (TOC%) and dry bulk density, alongside well constrained age models, from 81 sites of the International Ocean Discovery Program (IODP, Fig. 1). Further, we employ an algorithm that propagates the data from discrete, individual sites to biogeochemical "provinces" and then eventually, to the global ocean. This novel bottom-up approach is used to build continuous records of regional and global OC burial in the Miocene (~23-5.33 Ma) and Pliocene (~5.33-2.58 Ma) epochs, offering unique insights into the long-term global carbon cycle and the organic sub-cycle over this critical interval that helped shape our modern world.

Spatial variation of OC burial

We screened 1508 IODP sites (Site 1 to Site U1508) and identified 81 sites to establish mass accumulation rates (MARs) of TOC covering either a large portion or the entirety of the past 23 Myr (Fig. 2, Methods). When small temporal gaps were found, data from nearby sites, often drilled during the same expedition, were used to build a composite record (see Methods). MAR of OC at each site relies on reported TOC wt% and dry bulk density of the sediments compiled and calculated from the IODP database, and sedimentation rates calculated from the age-depth relationship of each site. We compared TOC% results obtained from the standard IODP "subtraction" method and the "acidification" method which presumably yields more accurate results, as well as results obtained during different phases of IODP operations (DSDP, ODP and IODP) from nearby sites, which broadly support the robustness of IODP's TOC% data (Extended Data Fig. 1, 2, Methods). All age models were updated to the GTS2012 (Ref [20]) timeframe (Methods).

The inherent unsteadiness of depositional systems often results in a negative power-law relationship between measurements of sedimentation rate and the amount of time averaged to determine the rate, independent of the sedimentary depositional environment[21]. To evaluate whether our OC burial rates were affected by this "Sadler effect", we compared the averaging interval (duration of time between tie-points in an age model), sediment accumulation, and OC burial for each record to determine the potential for spurious patterns to arise in our global OC burial flux reconstruction (Methods, Extended Data Fig. 3). These results suggest that our global OC MAR records are largely free of the Sadler effect and therefore represent realistic sedimentary OC burial changes over time.

Many factors impact the rate of OC burial, for example, the evolution of primary producers in the ocean and on land[22], marine primary and export productivity[23], bottom water oxygen levels and exposure time[24, 25], sea-level[24], sediment composition[26] and accumulation rates[27], the evolution of sediment bioturbators[28], and the activity of the microbes that break down organic matter[12]. Although our data cannot address all potential factors impacting OC burial, the spatial variability of OC burial rates over different time slices of Neogene indicates that the highest OC burial occurs on continental shelves, coastal seas and deep-sea sediment fans, consistent with the notion that enhanced production and preservation at these places contribute to high OC accumulation rates[22] (Extended Data Fig. 4).

Temporal variations of the global OC burial

To build global OC burial from 81 discrete records, we utilized an algorithm following a study that explored global OC burial since the last glacial period[29]. First, the world's ocean was divided into different provinces based on modern biogeochemical zonation. A simplified version of the ecological geography of Longhurst[30] was employed, with the caveat that biogeochemical zonation is potentially subject to changes over time (Extended Data Table 1). The definition of Longhurst provinces was based on atmospheric circulation, light, coastlines, water colum stratification, chlorophyll content and other environmental factors[30] and has been widely applied in marine biogeochemistry studies. We also explored other approaches to define the provinces, for example, the International Hydrographic Organization Sea Areas, and the Fishing Areas by the Food and Agriculture Organization of the United Nations (Methods and Extended Data Fig. 5) to test the sensitivity of the results to different choices of the provincial definition. Second, we obtained the modern global and hence provincial OC burial in marine sediments based on estimates derived from satellite and core-top data[31] (Extended Data Fig. 6). Third, the 81 individual TOC MAR records were used to construct relative changes of provincial variability of OC burial (Fig. 2). There is at least one, but often more records to represent each province (Extended Data Table 1).

An inherent issue of reconstructing global OC burial is the spatial offset between the presumably largest burial flux in shallow waters, and available continuous sedimentary records in relatively deeper waters (> 500 m). Our approach of using individual records from IODP sites to represent provincial OC burial helps to alleviate this problem. Also, most of the sediment load transported by large rivers does not accumulate on the deltaic area over the long term. This is shown by no major seaward growth of the subaerial delta over decades to centuries of the rivers with the highest sediment discharge such as the Ganges-Brahmaputra, Amazon, and Yellow Rivers[32]. Gravity drives the fine-grained sediment to be transported off the delta and shelf, usually initiated by sediment flux convergence and subsequently supported by wave and current-induced suspension[33]. This is exemplified by the Ganges-Brahmaputra River, the world's largest sediment dispersal system, which is highly effective in transporting sediment to the Bengal Fan bypassing the river delta. The suspended sediment can be found throughout the entire 3,000 km long, 1,000 km wide submarine fan[32] , the record of which is captured by Sites 758 and U1451 in our dataset.

Importantly, sedimentary organic matter degrades over time. Studies on the decay of organic matter observed a general relationship between the decomposition rate (k) and age of the sediment (t), given by $\log k = -0.95 \log t - 0.81$ (ref [34]). This relationship predicts that only ~4% of the original sedimentary OC (100%) is still preserved in one-million-year-old sediments. Since the current data and theory of OC decomposition is limited to the late Pleistocene, this relationship therefore cannot be directly extrapolated to the entire Neogene. Nevertheless, the rate of degradation levels off quickly after a few million years. As a result, we averaged the OC burial data between 2.5-0.5 Ma at each site and defined this as "modern burial" (Extended Data Fig. 6), following the common practice of many carbon cycle studies that treat the Pleistocene mean value as "modern"[1, 2]. For all IODP sites, their Neogene OC burial variabilities are relative to this "modern" value. As a reference, the modern OC burial in the global ocean is estimated to be 0.15 Gt C yr^{-1} (Ref [31]).

Our calculated OC burial rates for the global ocean (Fig. 3a) exhibit large fluctuations, with the highest fluxes found in the early Miocene and Pliocene, and lowest in the mid-Miocene. The highest OC burial rate in our record (~4 Ma) is about 0.23 ± 0.019 (1σ) Gt C yr^{-1}, which is roughly 1.8 times greater than the lowest OC burial rate, which occurred around ~13.5 Ma and was 0.083 ± 0.011 Gt C yr^{-1}. When cast in terms of the relative rate of OC burial over time, our data suggest variations between about 0.5 and 1.5 times the present-day rate.

In contrast, global biogeochemical models predict much smaller variations in OC burial rates. The COPSE model calculates organic fluxes using built-in nutrient cycles[7], where the oceanic concentrations of phosphate and nitrate control primary productivity and hence OC burial. A different approach is used in GEOCARBSULFOR, which derives organic fluxes from the isotopic records of carbon and sulfur using the isotope mass balance approach detailed earlier (e.g., Eq. 1 and 2)[8]. Both models predict OC burial rate variations within only 10% of the present-day rate, less than one quarter of the actual variation we show, and they tend to predict higher OC burial rates in the mid-Miocene whereas our new record shows a much reduced rate (Fig. 3b). A closer match to our data is seen in the inverse carbon cycle model of Li and Elderfield[9], which uses the Sr, Os and C isotope systems to back-calculate weathering and burial fluxes. Even though this approach estimates a greater degree of variation in OC burial than the more tightly coupled GEOCARBSULFOR and COPSE models, it is still substantially less than shown in our data (around 0.7 - 0.95 versus our range of around 0.5 - 1.5, Fig. 3b).

Reassessing the Neogene carbon cycle

The residence time of dissolved inorganic carbon in the ocean is on the order of 10^5 years[35]. On longer timescales, a change in the global organic carbon reservoir, arising on account of a persistent change in the proportion of carbon that is stored as organic carbon rather than as carbonate, must induce a shift in the global mean ^{13}C content of the carbonate that is being stored, assuming the input of carbon to the surficial system does not change[35]. Thus, the long-lasting positive carbon isotope excursion between 17-13.5 Ma (early to middle Miocene) is thought to be related to the Monterey Formation found in California and other widespread organic-rich sediment deposition around the rim of the Pacific Ocean. The lower section of the Miocene Monterey Formation commonly has calcareous facies with abundant mudstones and shales, followed by the mid-Miocene phosphatic facies, which are organic rich and coincide with the positive excursions of benthic $\delta^{13}C$ (Ref [36, 37, 38]). This is the basis for the supposition that a large quantity of OC could have been buried during this time. The famous "Monterey

Hypothesis" links this enhanced OC burial to the subsequent drop in atmospheric CO_2, global cooling and Antarctica glaciation observed in the middle Miocene climate transition[11, 39].

However, when OC burial rates for the Monterey Formation were quantified from the El Capitan State Beach, where TOC was abundant and varied between 1.2 and 23.2 wt%, average OC burial rate is only 0.23 mg cm^{-2} yr^{-1} between 16.3 -12.7 Ma, with the peak averaged rate of 0.39 mg cm^{-2} yr^{-1} found between 14.5 to 13.3 Ma, and the lowest of 0.04 mg cm^{-2} yr^{-1} during 13.3-12.7 Ma[37]. These low accumulation rates are primarily due to low sedimentation rates, such that the OC burial near California is directly comparable with our open ocean sites. For example, in the eastern equatorial Pacific, the average "Monterey period" (17-13.5 Ma) burial rates are 0.14 mg cm^{-2} yr^{-1} at Site 1337 and 0.19 mg cm^{-2} yr^{-1} at Site 1338. When all three records are compared over the same time interval (16.3-12.7 Ma), the Monterey Formation at El Capitan (0.23 mg cm^{-2} yr^{-1}) is indistinguishable from the equatorial upwelling region (Site 1338, 0.22 mg cm^{-2} yr^{-1}), but records much lower burial rates than the deep-sea sedimentary fans (Bay of Bengal, Site U1451, 6.5 mg cm^{-2} yr^{-1}, Extended Data Fig. 7). These quantitative analyses further argue against the conclusion that massive OC burial occurred near the Pacific rim during the "Monterey period" and is therefore responsible for the positive $\delta^{13}C$ excursion.

A simple interpretation of the positive $\delta^{13}C$ excursion recorded in benthic foraminifera (Fig. 4b) during the mid-Miocene (i.e., due to enhanced OC burial) does not consider potential changes in the input of carbon to the surficial system, in terms of both flux and isotopic composition. The $\delta^{13}C$ of atmospheric CO_2, reconstructed by benthic foraminiferal $\delta^{13}C$ from regions that presumably maintain close air-sea carbon exchange, i.e., areas with deep-water formation, provides important insights into possible changes in the source of atmospheric CO_2 (Ref [40]). During the mid-Miocene, this record exhibits the most positive values (between –5.5 and -5‰) of the entire Neogene (Fig. 4c), highlighting the potential contribution of isotopically heavy CO_2 to the atmosphere.

Volcanic outgassing of CO_2 represents a more ^{13}C-enriched source of atmospheric CO_2 in the long-term carbon cycle relative to OC weathering. During the mid-Miocene, the Columbia River flood basalt erupted in the northwestern United States. This volcanism peaked between 17-14.5 Ma[41, 42]. Because of its link to the subducted Farallon plate, the Columbia River Basalt Group (CRBG) is particularly rich in volatiles. 494,000 Gt of basalt produced during this period is estimated to have resulted in 4,090-5,670 Gt of carbon release[43]. This volcanic outgassing contributed to the positive excursion in the $\delta^{13}C$ of atmospheric CO_2, increased CO_2 levels, and caused global warming during the mid-Miocene. Such a scenario is supported by reconstructions of seawater chemistry, which showed a major increase in dissolved inorganic carbon in surface seawater due to the addition of volcanic CO_2 (Ref [44]), as well as by climate-biogeochemical cycle modelling[45]. Interestingly, our results show that reduced OC burial in the global ocean would act as an additional mechanism contributing to elevated CO_2 and therefore global warming during the mid-Miocene (Fig. 4a, d, e).

Our global OC burial data can also be used together with estimates of carbonate burial[46] to evaluate the ratio between organic and inorganic carbon burial in the global ocean. Current estimates of carbonate burial rely on a depth-dependent $CaCO_3$ preservation profile based on carbonate compensation depth (CCD) reconstructions or mass balance for carbonate alkalinity[46]. Our calculated organic vs. inorganic burial ratio reaches a minimum during the mid-Miocene, in particular, the Monterey period (Fig. 4g).

Assuming steady state in the long-term carbon cycle (Equation 1 and 2), we can also evaluate the history of the carbon input flux during the Neogene. The carbon isotopic composition of bulk organic matter[47] and carbonates[48] further enables us to compute the $\delta^{13}C$ of this carbon input. The calculated $\delta^{13}C$ of the carbon input shows large variations throughout the Miocene, particularly during the mid-Miocene with a large positive shift from about 19 Ma, peaking at around 14 Ma, with the calculated value from -5 to 0 ‰ (Fig. 4h). Similarly, the calculated total flux of carbon input presents clear variations over the Neogene (Fig. 4g). These substantial changes invoked for the carbon input and its isotopic values call for some fundamental revisions of how we view the global carbon cycle through this period of Earth history. Improved global carbon cycle models should be expected to include an organic sub-cycle that is highly variable, and the amount and isotopic composition of total carbon input to the surficial system should also evolve with time.

OC burial as positive feedback for the global climate

Although the controls on global OC burial are determined by many physical, chemical, biological and geological conditions and the interactions between them, reduced burial during the warmest phase of the past 23 million years might not be a coincidence. It is well known that the temperature-dependent metabolic rates of heterotrophic bacteria result in high rates of organic matter remineralization in a warmer water column, and therefore less carbon burial[49]. The metabolic activity of the microbes breaking down organic matter responds to temperature dramatically, with metabolic rates doubling for every 10°C-temperature increase, known as the Q10 pattern[12, 13, 50]. Bacterial changes are much more sensitive to warming than photosynthesis rates of primary producers, which leads to more efficient remineralization of sinking organic matter and less OC buried in the sediments[12]. Metabolic rate change has been invoked to explain the elevated efficiency of organic matter recycling in warm climates and reduced OC burial[49, 51].

The biological pump that is responsible for sending OC to the deep ocean, and ultimately sediments, has been evaluated for its strength by using the depth habitat and stable isotopes of planktonic foraminifera. Recent results suggest a much weaker biological pump during the Eocene greenhouse climate[51] and the warm mid-Miocene[13]. After 15 Ma, with the declining temperatures of the ocean, the deep-dwelling planktonic foraminifera greatly expanded their depth-habitat. These data, together with reconstructed $\delta^{13}C$ gradients in the water column and an Earth System modeling, were used to reveal a 2-4 times increase in the particulate organic matter flux to the mid-twilight zone over the past 15 million years[13]. This exemplifies how changes in temperature-dependent metabolic rates have influenced the ocean carbon cycle, consistent with our global OC burial data.

Our study quantitatively evaluates OC burial in the global ocean from the bottom-up, and demonstrates unforeseen variability of this important component of the global carbon cycle. The relationships between the organic carbon cycle and atmospheric CO_2 and O_2 levels are understudied, as demonstrated by the mismatch between our findings and popular carbon cycle models. Changes of OC burial over time as constrained by this study and future studies should be incorporated into subsequent analyses of the global carbon cycle. Our results support the notion that the greatly reduced OC burial during the warm period of the Miocene is related to the temperature dependence of bacterial metabolism that remineralizes organic matter, establishing positive feedback which increases atmospheric CO_2 as the climate warms. This feedback mechanism is expected to operate during other warming intervals over Earth history, as well as future warming of the global ocean.

Acknowledgement Acknowledgment is made to the donors of the American Chemical Society Petroleum Research Fund (59797-DNI2 to Y.G.Z.) for support of this research. Z.Y.L.'s visit to Texas A&M University was supported by the International Cooperative Program for Innovative Talents through China Scholarship Council Grant No. 201600090202. B.J.W.M is funded by the UK Natural Environment Research Council (NE/S009663/1). We thank Shuang Zhang for helpful discussions, Johan Renaudie and Dave Lazarus at the Neptune Database by providing biostratigraphy data for many sites used in this study, and John Dunne for providing the modern OC burial data. We also acknowledge the International Ocean Discovery Program, its funding agencies, and scientists around the world for generating the IODP data and making it available. Y.G.Z. conceived this idea onboard IODP Expedition 363 and therefore acknowledges the scientists and crew of that cruise, especially his fellow shipboard organic geochemist Masanobu Yamamoto for their diligent work and stimulating conversations. We thank the two anonymous reviewers for their thoughtful comments that helped to improve the quality of this article.

Author contributions Y.G.Z. designed this study. Z.Y.L. collated, analyzed and interpreted the data to establish OC burial records, with input from Y.G.Z. M.T. evaluated the records for "Sadler Effect" and B.J.W.M. ran the carbon cycle models. All authors contributed to the writing, led by Z.Y.L. and Y.G.Z.

Competing interests The authors declare that they have no competing interests.

Correspondence and request for materials should be addressed to Yi Ge Zhang (yige.zhang@tamu.edu).

Cited References

1. Berner RA. Burial of organic carbon and pyrite sulfur in the modern ocean: Its geochemical and environmental significance. *Am J Sci* 1982, **282:** 451-473.

2. Hedges JI, Keil RG. Sedimentary organic matter preservation: an assessment and speculative synthesis. *Mar Chem* 1995, **49:** 81-115.

3. Broecker WS. A new boundry condition on atmospheric oxygen. *J Geophys Res* 1970, **75:** 3553-3557.

4. Garrels RM, Lerman A. Coupling of the sedimentary sulfur and carbon cycles - An improved model. *Am J Sci* 1984, **284:** 989-1007.

5. Derry LA, France-Lanord C. Neogene growth of the sedimentary organic carbon reservoir. *Paleoceanography* 1996, **11:** 267-276.

6. Kump LR, Arthur MA. Interpreting carbon-isotope excursions: carbonates and organic matter. *Chem Geol* 1999, **161:** 181-198.

7. Mills BJW, Krause AJ, Scotese CR, Hill DJ, Shields GA, Lenton TM. Modelling the long-term carbon cycle, atmospheric CO_2, and Earth surface temperature from late Neoproterozoic to present day. *Gondwana Research* 2019, **67:** 172-186.

8. Krause AJ, Mills BJW, Zhang S, Planavsky NJ, Lenton TM, Poulton SW. Stepwise oxygenation of the Paleozoic atmosphere. *Nat Commun* 2018, **9:** 4081.

9. Li G, Elderfield H. Evolution of carbon cycle over the past 100 million years. *Geochim Cosmochim Acta* 2013, **103:** 11-25.

10. Flower BP, Kennett JP. The middle Miocene climatic transition: East Antarctic ice sheet development,

deep ocean circulation and global carbon cycle. *Palaeogeogr Palaeoclimatol Palaeoecol* 1994, **108:** 537-555.

11. Vincent E, Berger WH. Carbon dioxide and polar cooling in the Miocene: The Monterey hypothesis. In: Sundquist ET, Broecker WS (eds). *The carbon cycle and atmospheric CO2: Natural variations Archaen to Present*, vol. 32. AGU: Washington, DC, 1985, pp 455-468.

12. Regaudie-de-Gioux A, Duarte CM. Temperature dependence of planktonic metabolism in the ocean. *Global Biogeochem Cyc* 2012, **26:** GB1015.

13. Boscolo-Galazzo F, Crichton KA, Ridgwell A, Mawbey EM, Wade BS, Pearson PN. Temperature controls carbon cycling and biological evolution in the ocean twilight zone. *Science* 2021, **371:** 1148-1152.

14. Shields GA, Mills BJW. Tectonic controls on the long-term carbon isotope mass balance. *Proceedings of the National Academy of Sciences* 2017, **114:** 4318-4323.

15. Bolton EW, Berner RA, Petsch ST. The weathering of sedimentary organic matter as a control on atmospheric O2: II. Theoretical modeling. *Am J Sci* 2006, **306:** 575-615.

16. Torres MA, West AJ, Li G. Sulphide oxidation and carbonate dissolution as a source of CO_2 over geological timescales. *Nature* 2014, **507:** 346-349.

17. Mason E, Edmonds M, Turchyn AV. Remobilization of crustal carbon may dominate volcanic arc emissions. *Science* 2017, **357:** 290-294.

18. Bradbury HJ, Turchyn AV. Reevaluating the carbon sink due to sedimentary carbonate formation in modern marine sediments. *Earth Planet Sci Lett* 2019, **519:** 40-49.

19. Schrag DP, Higgins JA, Macdonald FA, Johnston DT. Authigenic carbonate and the history of the global carbon cycle. *Science* 2013, **339**(540-543).

20. Gradstein FM, Ogg JG, Schmitz M, Ogg G. *The geological time scale 2012*. Elsevier, 2012.

21. Sadler PM. Sediment accumulation rates and the completeness of stratigraphic sections. *Journal of Geology* 1981, **89:** 569-584.

22. Berner RA. Examination of hypotheses for the Permo-Triassic boundary extinction by carbon cycle modeling. *Proc Natl Acad Sci* 2002, **99:** 4172-4177.

23. Pedersen TF, Calvert SE. Anoxia vs. productivity: What controls the formation of organic-carbon-rich sediments and sedimentary rocks? *AAPG Bulletin* 1990, **74:** 454-466.

24. Arthur MA, Sageman BB. Sea level control on source rock development: Perspectives from the Holocene Black Sea, the mid-Cretaceous Western Interior Basin of North America, and the Late Devonian Appalachian Basin. In: Harris NB (ed). *The deposition of organic carbon-rich sediments: Models, mechanisms and consequences*. Society for Sedimentary Geology: Tulsa, OK, 2005.

25. Hartnett HE, Keil RG, Hedges JI, Devol AH. Influence of oxygen exposure time on organic carbon preservation in continental margin sediments. *Nature* 1998, **391:** 572-574.

26. Lalonde K, Mucci A, Ouellet A, Gelinas Y. Preservation of organic matter in sediments promoted by iron. *Nature* 2012, **483:** 198-200.

27. Ingall EA, Van Cappellen P. Relation between sedimetnation rate and burial of organic phosphorus and organic carbon in marine sediments. *Geochim Cosmochim Acta* 1990, **54:** 373-386.

28. Boyle RA, Dahl TW, Dale AW, Shields-Zhou GA, Zhu M, Brasier MD*, et al.* Stabilization of the coupled oxygen and phosphorus cycles by the evolution of bioturbation. *Nature Geosci* 2014, **7**(9)**:** 671-676.

29. Cartapanis O, Bianchi D, Jaccard SL, Galbraith ED. Global pulses of organic carbon burial in dee-sea sediments during glacial maxima. *Nat Commun* 2016, **7:** 10796.

30. Longhurst AR. *Ecological geography of the sea.* . Elsevier, 2010.

31. Dunne JP, Hales B, Toggweiler JR. Global calcite cycling constrained by sediment preservation controls. *Global Biogeochem Cyc* 2012, **26:** GB3023.

32. Kuehl SA, Hariu TM, Moore WS. Shelf sedimentation off the Ganges-Brahmaputra river system: Evidence for sediment bypassing to the Bengal fan. *Geology* 1989, **17:** 1132-1135.

33. Wright LD, Freiedrichs CT. Gravity-driven sediment transport on continental shelves: A status report. *Cont Shelf Res* 2006, **26:** 2092-2107.

34. Middlelburg JJ, Vlug T, Jaco F, Van der Nat W. Organic matter reminderalization in marine systems. *Global Planet Change* 1993, **8:** 47-58.

35. Shackleton NJ. The carbon isotope record of the Cenozoic: History of organic carbon burial and of oxygen in the ocean and atmosphere. In: Brooks J, Fleet AJ (eds). *Marine petroleum source rocks*, vol. 26. Geological Society Special Publication: London, UK, 1987, pp 423-434.

36. Compton JS, Snyder SW, Hodell DA. Phosphogenesis and weathering of shelf sediments from the southeastern United States: Implications for Miocene d13C excursions and global cooling. *Geology* 1990, **18:** 1227-1230.

37. John CM, Follmi KB, De Kaenel E, Adatte T, Steinmann P, Badertscher C. Carbonaceous and phosphate-rich sediments of the Miocene Monterey Formation at El Capitan State Beach, California, U.S.A. *Journal of Sedimentary Research* 2002, **72:** 252-267.

38. Follmi KB, Badertscher C, de Kaenel E, Stille P, John CM, Adatte T*, et al.* Phosphogenesis and organic-carbon preservation in the Miocene Monterey Formation at Naples Beach, California-The Monterey hypothesis revisited. *GSA Bull* 2005, **117:** 589-619.

39. Thomas E, Vincent E. Equatorial Pacific deep-sea benthic foraminifera: Faunal changes before the middle Miocene polar cooling. *Geology* 1987, **15:** 1035-1039.

40. Tipple BJ, Meyers SR, Pagani M. Carbon isotope ratio of Cenozoic CO_2: A comparative evaluation of available geochemical proxies. *Paleoceanography* 2010, **25:** PA3202.

41. Hodell DA, Woodruff F. Variations in the strontium isotopic ratio of seawater during the Miocene: Stratigraphic and geochemical implications. *Paleoceanography* 1994, **9:** 405-426.

42. Kasbohm J, Schoene B. Rapid eruption of the Columbia River flood basalt and correlation with the mid-Miocene climate optimum. *Science Advances* 2018, **4:** eaat8223.

43. Lange RA. Constraints on the preeruptive volatile concentrations in the Columbia River flood basalts. *Geology* 2002, **30:** 179-182.

44. Sosdian S, Babila T, Greenop R, Foster G, Lear C. Ocean Carbon Storage across the middle Miocene: a new interpretation for the Monterey Event. *Nat Commun* 2020, **11**(1)**:** 1-11.

45. Longman J, Mills BJW, Donnadieu Y, Godderis Y. Assessing volcanic controls on Miocene climate change. *Geophys Res Lett* 2022, **49:** e2021GL096519.

46. Boudreau BP, Luo Y. Retrodiction of secular variation in deep-sea $CaCO_3$ burial during the Cenozoic. *Earth Planet Sci Lett* 2017, **474:** 1-12.

47. Falkowski PG, Katz ME, Milligan AJ, Fennel K, Cramer BS, Aubry M-P*, et al.* The rise of oxygen over the past 205 million years and the evolution of large placental mammals. *Science* 2005, **309:** 2202-2204.

48. Katz ME, Wright JD, Miller KG, Cramer BS, Fennel K, Falkowski P. Biological overprint of the geological carbon cycle. *Mar Geol* 2005, **217:** 323-338.

49. Olivarez Lyle A, Lyle M. Missing organic carbon in Eocene marine sediments: Is metabolism the biological feedback that maintains end-member climates. *Paleoceanography* 2006, **21**.

50. Stanley SM. Relation of Phanerozoic stable isotope excursions to climate, bacterial metabolism, and major extinctions. *Proceedings of the National Academy of Sciences* 2010, **107:** 19185-19189.

51. John EH, Wilson JD, Pearson PN, Ridgwell A. Temperature-dependent remineralization and carbon cycling in the warm Eocene oceans. *Palaeogeogr Palaeoclimatol Palaeoecol* 2014, **413:** 158-166.

Fig. 1 | Location of our studied sites overlaid on the Longhurst biogeochemical provinces. The Longhurst map defines 56 coherent provinces from the modern biogeochemistry perspective[30], which were simplified to 27 provinces used in this study (Extended Data Table 1). The original provinces were merged based on their geographical proximity and biogeochemical similarity, to ensure that each new province is represented by at least one site over the Neogene. Different shapes and colors denote IODP (International Ocean Discovery Program and Integrated Ocean Drilling Program, red diamonds), ODP (Ocean Drilling Program, maroon dots) and DSDP (Deep Sea Drilling Project, blue squares) sites.

Fig. 2 | Provincial OC burial changes and their contribution to the global OC burial. a. Relative changes of provincial OC burial rates over time, with the "modern" (Pleistocene) value defined as 1; **b.** Provincial contribution to the global OC burial rates during the Neogene (total = 100%), with the leftmost column representing the modern burial of Dunne et al.[31]. The provinces presented here are identical to those shown in Fig. 1. Refer to Extended Data Table 1 for the details of each province and the IODP sites used to construct provincial records.

Fig. 3 | Neogene OC burial in the global ocean. a. Burial rates calculated using different definitions of provinces, including Longhurst (black curve with uncertainty envelope, $\pm 1\sigma$ in purple and $\pm 2\sigma$ in pale lilac), Oceans (blue curve), and FAO Fishing (orange curve) approaches. **b.** Comparisons of global OC MAR between our record and the output of commonly used global carbon cycle models (COPSE[7], GEOCARBSULFOR[8], and Li & Elderfield[9]). All relative changes were normalized to the "modern" (Pleistocene) level.

Fig. 4 | Neogene climate and carbon cycle changes. **a.** A stacked deep-sea benthic foraminiferal $\delta^{18}O$ curve[52] **b.** Benthic $\delta^{13}C$ stack[52]. **c.** 3 Myr moving average of $\delta^{13}C_{CO2}$ (Ref [40]). **d.** Atmospheric CO_2 reconstructions based on marine proxies including the alkenone (green hollow squares) and boron (solid blue squares) methods[53]. Sky blue line is the LOESS fit curve. **e.** Neogene OC burial in the global ocean with $\pm 1\sigma$ uncertainty envelope. **f.** Ratio between organic carbon and carbonate carbon burial (OC: IC). Carbonate burial[46] was calculated based on two CCD scenarios. **g.** Calculated flux of total carbon input to Earth's surficial system. Absolute burial rates were adjusted to match the assumption that the "modern" (2.5-0.5 Ma) burial ratio between inorganic and organic carbon is 4:1. **h.** Calculated $\delta^{13}C$ of the total carbon input to Earth's surficial system. The changing inorganic vs. organic burial ratio during the Neogene, together with $\delta^{13}C_{IC}$ (Ref [48]) and $\delta^{13}C_{org}$ (Ref [47]) data were used to obtain this record though Equation 2. Pink and blue vertical bars highlight the timing of the Miocene Climatic Optimum (MCO) and Middle Miocene Climate Transition (MMCT).

Methods

Methods Overview

Building upon a study that reports global ocean OC burial variability since the last glacial period[29], our calculation of global organic carbon burial fluxes over the Neogene (23.0-2.6 Ma) period involves a series of consecutive steps. First, we screened 1508 sites from the Deep Sea Drilling Project (DSDP, Leg 1-96), Ocean Drilling Program (ODP, Leg 100-210), Integrated Ocean Drilling Program (IODP, Exp 301-312), and International Ocean Discovery Program (IODP, Exp 317-363). Out of the 1,490 sites, 81 sites were identified (Fig. 1) with available total organic carbon concentrations (TOC%), dry bulk density, and age model datums covering most of the past 23 million years. These sites span all major ocean basins and depositional environments, including regions with large terrestrial sediment input, areas with strong upwelling activity and associated high rates of primary productivity, and pelagic, carbonate-rich, open ocean areas, and so on.

The mass accumulation rates (MARs) of organic carbon (OC) were calculated for each site based on sedimentation rate, bulk density, and TOC%. Individual TOC MARs were then used to determine the spatial and temporal variability of regional and global OC burial in the Neogene. Extended Data Fig. 8 provides an example to show the workflow of building TOC MARs from TOC%, bulk density and age-depth relationship data.

To build the global burial OC fluxes from the 81 individual records, we subdivide the world ocean into different biogeochemical provinces. The modern burial flux for each province, which is used to scale our paleo-data, was estimated based on a series of algorithms and data from core-top sediments and satellites[54]. Given the inherent bias introduced by any such division, we employed three different subdivision strategies (Fig. 1; Extended Data Fig. 5a, b) and compared the results to assess the uncertainty of our global reconstruction.

Previous work has identified potential biases in flux reconstructions that make use of sedimentation rate as a result of the Sadler Effect[21, 55]. Simply, the inherent unsteadiness of depositional systems results in a negative power-law relationship between measurements of sedimentation rate and the amount of time averaged to determine the rate independent of the sedimentary depositional environment[21]. To evaluate the potential impact of the Sadler Effect on our reconstruction, we compared the averaging interval (duration of time between tie-points in an age model), sedimentation accumulation, and OC burial for each record to determine the potential for spurious patterns to arise in our global OC burial flux reconstruction (see section on Sadler Effect analysis below).

Site Selections

Sediment cores from DSDP/ODP/IODP are our best archive for obtaining continuous records with well-established chronology. Sediment from pelagic or hemipelagic sites would also, to some extent, reduce the potential bias from turbidite sequences. We went through all Initial Reports volumes up through IODP Expedition 363 to select sites suitable for this study.

Drilled sites must have sufficient quantity and quality of data to be included in our compilation, with both complete or near complete sediment sections cored for the last 23 Myr, as well as a reliable age model, TOC% and sediment bulk density data for the Neogene.

Age Models

Several independent approaches are often used by DSDP/ODP/IODP to provide constraints on the chronology of sediment cores. These methods include biostratigraphy (planktonic foraminifer, benthic foraminifer, calcareous nannofossils, diatoms, and radiolarians) and magnetostratigraphy (geomagnetic polarity reversals). A major issue with age models published in the past few decades is that they are based on different absolute timeframes of magnetic reversal or bio-horizon events. Recent advances in radiometric dating, orbital tuning and the understanding of stratigraphic relationships are reflected by the more recent Geological Timescale 2012 (GTS 2012) (ref. [20]). As such, we converted all reported magnetochrons and microfossil biochronology at our study sites to the GTS 2012 timescale so that comparisons between records and the stacking of records to obtain a regional and global picture of OC deposition are referring to the same chronological framework. Most of the IODP/ODP sites we used in this study have their age tie points readily available. However, for sites where the initial reports and/or associated publications do not provide detailed age-depth relationships (most DSDP sites), we consulted the Neptune database[56, 57] to obtain the biostratigraphic data.

Sedimentation Rates

Sedimentation rate for each site was determined by performing a 3rd-6th order polynomial regression to the age-depth relationship (Extended Data Fig. 8), followed by the calculation of the first order derivative of this relationship. Generally, the higher order of polynomial fitting would result in better fitting reflected by the r^2 values close to one. But we are aware of the possibility of over-fitting. Our strategy was that among all regressions with certain conditions (i.e., r^2 greater than 0.90 and fitting residuals that do not vary systematically with age), the lowest order polynomial equation was selected to represent the age-depth relationship. Our polynomial regression captures these relationships well, reflected by the r^2 values from all sites ranging from 0.9185 to 0.9995 with a mean value of 0.9882 and 1σ of ± 0.0015.

Dry Bulk Density and TOC%

Dry bulk density (DBD) measurements are performed by shipboard physical property specialists, with the data presented in the "Physical Properties" section of the initial site reports. TOC% are determined by shipboard geochemists. These data are published in "Geochemistry", "Organic Geochemistry" or "Carbon Geochemistry" section of the initial site reports. They are available as tables associated with the site report or can be found online through the "Janus" database for Expedition 1-312, or the "LIMS" database for Expedition 317 - present. Because some DSDP sites only reported bulk density (BD) but not dry bulk density data, we developed an empirical equation with statistical significance based on a linear correlation between DB and DBD ($R^2 = 0.9995$), using 842 data points from 10 IODP sites where both type of measurements are available:

$$DBD = 1.5441 \times BD - 1.5458 \qquad \text{Equation 3}$$

The Quality of IODP's TOC% Data

DSDP/ODP/IODP use a standard "subtraction" method onboard of the R/V to determine TOC%, which is based on the differences between the total carbon measured by a CHNS elemental analyzer (EA) and the inorganic carbon measured by a coulometer. This method is generally considered to be accurate. For example, Meyers and Silliman[58] replicated the ship-board TOC% measurements by performing shore-based experiments that removed the carbonate fraction of samples through acid digestion (i.e., "acidification method"). The residues were then washed, dried, and measured on an EA. Their shore-based results (0.06-3% TOC) were positively correlated with the shipboard values[58]. However, Olivarez Lyle and Lyle[59] argued that the subtraction method introduces large errors when TOC% is low (< 0.3%). By using carefully designed acid digestion method, Olivarez Lyle and Lyle[49] were able to report very low mean TOC concentrations of about 0.03% at Sites 1218 and 1219, levels that are "below detection" using the standard subtraction method[60]. In this case, acidification method clearly showed its advantage over the standard subtraction method when sediment samples bear very low TOC%. However, samples reportedly have “0%” or “below detection” of TOC constitutes only 2.5% of our database.

Several IODP publications attempted to evaluate of the accuracy of the standard “subtraction” method for determining TOC%[61, 62]. Here, we compiled all available TOC% data that have been constructed from both the “subtraction” and “acidification” methods and compare them downcore as well as scatter plot on the absolute abundance scale (Extended Data Fig. 1). Some offsets between the two datasets were observed. Nevertheless, the overall relationship suggests that the two independent methods yield comparable results (p-value = 1.38^{e-17}), supporting the robustness of the standard subtraction method for TOC% used by IODP.

Also, to determine the consistency of TOC% data reported by DSDP, ODP or IODP expeditions over several decades, we compared results found in nearby locations. To obtain more material for follow up studies, IODP expeditions occasionally revisit earlier DSDP or ODP site locations. Since their locations and water depth are almost identical, a direct comparison of TOC% on the depth scale of these sites was conducted (Extended Data Fig. 2). When the sites were not directly “revisited” but still drilled within a short distance and similar water depth, we used a criterion of <10 km apart and <200 m depth differences to identify sites suitable for such comparisons, with one exception of IODP U1341 and DSDP 188 that are slightly further apart but still bearing similar physical properties. For sites that are beyond this range, substantially different sedimentation rates would complicate any TOC% comparison on the depth scale. Extended Data Fig. 2 shows a broad agreement between DSDP, ODP and IODP-derived TOC% results, except for the Sites 716 - U1467 where the ODP results constantly represent the lower end of the IODP measurements. The resemblance of TOC% records from nearby sites but measured during different time periods demonstrates the long-term consistency of IODP’s TOC% data.

OC MAR Calculations

Mass accumulation rate (MAR) of OC is calculated by the equation:

$$\text{TOC MAR} = \text{SR} \times \text{TOC\%} \times \text{DBD} \qquad \text{Equation 4}$$

Where SR (cm kyr^{-1}) is the sedimentation rate, TOC% is the weight percentage of total organic carbon, and DBD is the dry bulk density (g cm^{-3}, grams of sediment per cubic centimeter of the original wet sample). If TOC% and DBD are not from the identical set of samples, then DBD data were interpolated to the depth of the TOC% data since DBD data usually have a higher sampling density. Extended Data Fig. 8 presents a working flow chart of IODP Site U1337, as an example to show how OC MAR data were obtained.

Sadler Effect Analysis

Apparent variations in sedimentation rate due to changes in the averaging interval (i.e., the duration of time between points in the age-depth relationship used to calculate sedimentation rate[21]) might contribute noise and/or bias in our reconstruction of OC MAR. If, for example, more recent portions of the core were characterized by higher resolution dating, then this could manifest as an artifactual increase in OC MAR due to differences in the averaging interval between younger and older portions of the record.

To assess whether changes in the averaging interval influence our ultimate conclusions about OC burial, we computed the expected changes in OC MAR that arise solely from changes in the averaging interval (i.e., the Sadler Effect) and compared these to our observations (Extended Data Fig. 3). To calculate the averaging interval for each depth in each core where we have an estimate of OC MAR, we identified the closest (in depth) age determinations above and below the OC MAR measurement and took the difference in age as a measure of the averaging interval. Using the power-law exponent for the relationship between averaging interval and sedimentation rate in Sadler (1981), we calculated a relative sedimentation rate for each measurement of OC MAR in each core. Using the same extrapolation algorithm used to calculate a global OC MAR (see below), we determine a global estimate of relative changes in sedimentation rate due solely to differences in the averaging interval with time. This time-series represents the pattern of changes in OC MAR that could arise artifactually.

In panels a and b of Extended Data Fig. 3, we show the range in averaging timescale between each core for a given age bin (i.e., the raw data used in the global extrapolation). This analysis shows a slight decrease in averaging interval towards the present (Extended Data Fig. 3a). However, differences in the distribution of averaging intervals between three time bins picked to capture the general U-shape trend in global OC MAR are too small to explain the factor of 2 changes in OC MAR apparent in our global reconstruction (Extended Data Fig. 3b). This result, along with the evidence that TOC%, and not sedimentation rate, is the dominant control on OC MAR for most sites (Extended Data Fig. 10), suggests that the patterns in our global OC MAR reconstruction reflect real changes during the Neogene and not solely spurious artifacts having to do with the complexities of the sedimentary record. This conclusion is further supported by comparing the global record of OC MAR to the global record expected based on spurious changes in sedimentation rate (Extended Data Fig. 3c, d). The poor correlation between the observations and the predictions using the Sadler Effect support the conclusion that the general U-shaped trend in OC MAR is a primary signal.

Apparent Controls of OC MARs

Geographically, regions like the Southwest African continental margin, Northwest Atlantic Ocean, Bay of Bengal, Antarctica margin (Wilkes Land) and Peru continental margin appear to be OC burial "hot spots" (Extended Data Fig. 4). Highly productive open ocean settings (e.g., upwelling regions in the eastern equatorial Pacific) do not show particularly high OC burial (Extended Data Fig. 4). In contrast, coastal-upwelling areas with high productivity and ample supply of terrigenous material have the ideal conditions for high OC burial rates[1], as exemplified by the Southwest African continental shelf and Peru continental margin. In the Bay of Bengal, high erosion rates of the Himalayas provided large amount of terrestrial organic matter and clastic material[63, 64], resulting in high sedimentation rate and rapid accumulation of OC (Extended Data Fig. 4). Of course, the geographical pattern discussed here are restricted spatially and temporally by the available IODP records with high quality and continuous TOC MAR records. Consequently, these records were used to scale for regional OC burial changes (Fig. 2) which reduces the sensitivity of calculated regional and global OC burial to any individual TOC MAR record.

To evaluate the apparent controlling factor of OC burial, we performed simple liner regression fittings between MAR and SR, TOC%, and DBD of each site. Importantly, SR and TOC% are interdependent – for example, rapid sedimentation dilutes OC flux, whereas quick burial potentially reduces the exposure time of OC to oxygen and therefore enhances the preservation of organic matter. Our analysis does not distinguish between these interconnections. The most significant correlation exhibited by the highest r^2 value was identified (Extended Data Fig. 9). The fitting results showed that TOC% exerts the largest control (68% of the sties) on MARs. In addition, 13.5% of the sites had OC MAR that were primarily influenced by changes in SR. Unclear controls were found in 18.5% of sites, implying a mixed influence. Our results show that TOC content appears to exert the dominant control of OC burial in a large number of sites, although TOC% itself is impacted by SR (Extended Data Fig. 9).

Provincial Definition Strategies

To infer regional/global patterns of OC burial changes from individual sites, we subdivided the world ocean into different sets of geographical provinces. Given the inherent bias introduced by any such subdivision, we adopted three different subdivision strategies (Fig. 1; Extended Data Fig. 5) and compared the results to test the dependence of our results on provincial definition.

Since the modern configuration of continents and oceans are largely in place during the Neogene, we utilized the Longhurst biogeochemical provinces of the modern ocean, assuming that the large-scale ocean features driving biogeochemical cycles have remained relatively stationary over time. The Longhurst biogeochemical map defines 56 coherent provinces, which was simplified into 27 provinces in our study (Extended Data Table 1) to adapt the ocean delineation to our site distribution.

To test how reliable regional and global OC burial records based on the Longhurst provinces are, we explored two other definitions. Very simply, we used the Arctic, Atlantic (South and North), Indian, Pacific (North, South, and Western) and Southern Oceans (Extended Data Fig. 5a), according to IHO Sea Areas, with version 3 retrieved from http://www.marineregions.org/. Another method is from FAO "Major Fishing Areas for Statistical Purposes", with the shapefiles retrieved from the FAO Fisheries and Aquaculture Department website, http://www.fao.org/fishery/area/search/en. FAO subdivided the Atlantic and Pacific Oceans into northwest, northeast, western central, eastern central, southwest, southeast and Antarctic regions. Also, the Indian Ocean was subdivided into western, eastern and Antarctic and Southern regions. Since there were no suitable sites for the Mediterranean and Black Sea, we combined the two areas into one conjoined province. Mercator projection for maps were used in both GMT and R.

Potential Water Depth Influence

As oceanic crusts move away from the spreading center (i.e., middle ocean ridges), they sink progressively. This implies that almost all our studied sites would be in shallower water depth during the Neogene than they are today. Using an observation-based empirical relationship ($D = 320 \times \sqrt{\mathrm{Age}}$, where 'D' is depth added and 'Age' is in million years) that is widely accepted[65], sites are estimated to be ~1,500 m shallower at 23 Ma. However, the relationship between water depth and OC burial rates is complicated and nonlinear. This is exemplified by analyses of our "modern" (Pleistocene) OC burial rates from the 81 sites and their modern water depth, which does not show any significant correlation. The linear regression yields result with $r^2 = 0.00000002$ and $p = 0.999$. Also, in contrast to time-induced water depth change that is monotonic, our reconstructed global OC burial record shows overall high, low and then high rates of organic burial over the Neogene (Fig. 3), arguing against a general water-depth control. Although the influence of water depth changes on our OC burial records is difficult to quantify, our approach of using one or more TOC MAR record(s) to scale for provincial changes helps to alleviate this potential issue. For 27 biogeochemical provinces used in this study, 21 of them have more than one TOC MAR record, often representing sites from different water depths (Extended Data Table 1).

Calculations of Regional and Global OC Burial

Modern OC burial in the global ocean with a 1×1° spatial resolution of Dunne et al.[31, 54] is the basis for our modern provincial OC burial rates, obtained from areal integrals of all data points within that province (Extended Data Fig. 6). This modern OC burial map is produced by a series of data and algorithms considering satellite-based primary production, particulate organic matter generation, transportation and burial in the sediments, which leads to a global burial of ~0.146 Gt C yr^{-1} (Ref [31, 54]). However, different methods have yielded drastically estimates of modern burial, possibly due to the fact that core-top samples could carry signals that are tens of thousands of years old but the sedimentation/remineralization rates were poorly constrained[66]. Nonetheless, recent studies utilized ^{230}Th-normalized fluxes to tackle this issue by minimizing age model uncertainties. For example, Hayes et al.[67] compiled results from 12,000 globally distributed marine cores and 1,068 flux estimates of the deep ocean. Their reported "deep water" (>2,000 m) annual OC burial of 0.017 ± 0.005 Gt C yr^{-1} is much more in line with Dunne et al. (2007, 2012) deep water burial rate of 0.012 Gt C yr^{-1}, supporting the robustness of the modern OC burial map used in this study.

Next, the ratio between TOC MARs of any Neogene interval and "Modern" (Pleistocene) of each site was calculated. If there are more than one site from any province, then these OC burial records were averaged to obtain the composite provincial changes. Subsequently, the absolute modern burial value of each province is multiplied by these ratios to determine provincial changes of OC burial over time. Finally, the sum of all provincial OC burial data provides the global OC accumulation rates. Mathematically, this approach can be written down as:

$$OC\ Burial_{(t)} = \sum_{p=1}^{27} m_p \cdot \left(\overline{OCV_{s,t}} \mid s \in p \right) \qquad \text{(Equation 6)}$$

where global OC burial at time t is the sum over all 27 provinces (Fig. 1, Extended Data Table 1) and OC burial in each province (p) is determined by the mean OC variability (OCV, with “modern” or 2.5-0.5 Ma defined as ‘1’) across all sites (s) within the province at the time t, multiplied by its modern provincial burial (m_p) (Extended Data Table 1). This approach also allows for easy adjustments if our understanding of the modern global burial further improves in the future.

For calculated global OC burial, the following equation was used to estimate the errors：

$$f = \sum_i^n a_i \sigma_{\bar{i}} \quad \text{Equation 7}$$

Where $\sigma_{\bar{i}}$ is the standard error of the OC burial change rate of each province, a is the modern provincial burial. Since modern OC burial values for each province are uncorrelated, the variance of *f* is therefore:

$$\sigma_f^2 = \sum_i^n a_i^2 \sigma_{\bar{i}}^{\ 2} \quad \text{Equation 8}$$

where

$$\sigma_f = \sqrt{\sum_i^n a_i^2 \sigma_{\bar{i}}^{\ 2}} \quad \text{Equation 9}$$

Extended Data Fig. 1 | Comparisons of TOC% obtained by “subtraction” method and “acidification” method. a-c. ODP Sites 897-899. **d.** IODP Site U1482. Navy blue squares are the measurements on board by subtraction between total and carbonate carbon contents, while blue dots are from the acidification method direct measured from carbonate-free samples. **e.** Linear regression of TOC contents determined by two independent methods. The regression equation is expressed as y = 0.8653*x, with $R^2 = 0.523$, p-value = 1.38^{e-17} and RMSE =0.593, suggesting a significant linear relationship at the 0.05 level of significance. The dashed grey line indicated the one-to-one correspondence of the two variables.

Extended Data Fig. 2 | Comparisons of TOC% reported by DSDP, ODP or IODP expeditions from nearby locations. a. IODP U1513 vs DSDP 258. **b.** IODP U1417 vs DSDP 178. **c.** IODP U1467 vs ODP 716. **d.** IODP U1327 vs ODP 889A. **e.** IODP U1341 vs DSDP 188. **f.** IODP U1424 vs ODP 794. **g.** ODP 904 vs DSDP 612. Site details are shown in Supplemental Data 10.

Extended Data Fig. 3 | Sadler effect evaluation. a. Changes in averaging intervals and their ranges between cores for 1 Ma time bins. The large black points show median values. The vertical black lines show the range from minimum to maximum averaging interval. The small grey points show the averaging intervals for individual cores in each time bin. The colored horizontal lines show the mean values for 3 age bins selected to capture the general U-shaped trend in OC MAR. **b.** Probability density functions of averaging intervals calculated for each core grouped into three age bins (>17.5 Ma, 10-17.5 Ma, and 2.5 to 10 Ma). **c.** Time-series of relative changes in global OC MAR (black) and global averaging interval (blue) expressed as a sedimentation rate using the power-law scaling of Sadler (1981). **d.** Scatter plot of global OC MAR and the global averaging interval expressed as a sedimentation rate showing a poor correlation.

Extended Data Fig. 4 | Individual site TOC MARs over four time slices during the Neogene. a. 20 Ma (early Miocene), **b**. 15 Ma (middle Miocene), **c**. 10 Ma (late Miocene), and **d**. 5 Ma (early Pliocene). Paleogeographic maps were reconstructed using Gplates software[68], with the sites rotated back to their paleo-locations. The contours of OC burial rate were obtained by performing IDW (Inverse distance weight function) interpolation of the data from individual sites (black dots, see Fig. 1 for site labels).

Extended Data Fig. 5 | Alternative approaches to define provinces of the world's ocean. a. IHO Sea Areas provinces. According to the IHO Sea Areas provinces zoning method, the global ocean is divided into the Arctic, Atlantic, Indian, Pacific and Southern Oceans. The Atlantic and Indian Oceans are further divided into the North and South Atlantic and the South, North and West Pacific, resulting in a total of 8 provinces. **b.** FAO Fishing Areas provinces. This method divides the global ocean into 19 geographical regions. Different shapes and colors indicate IODP (red diamonds), ODP (maroon dots), and DSDP (blue squares) site locations.

Extended Data Fig. 6 | "Modern" OC burial rates of the global ocean. The map was generated by data from Dunne et al. (2007, 2012). Also shown are "modern" (Pleistocene) burial rates of our 81 IODP sites (in diamond squares) color coded with the same scheme of the Dunne map.

Extended Data Fig. 7 | Comparing OC burial rates of different locations over several stages of the "Monterey period". OC accumulation rates for the Monterey Formation (EL Capitan) are compared with sites from the eastern equatorial Pacific (EEP, Site 1338), Bay of

Bengal (Site U1451), Southwest African continental Shelf (Site 362) and open ocean (Site 1335). Note that OC burial rates for the Monterey Formation are generally higher than the open ocean site, but lower than other sites.

Extended Data Fig. 8 | An example to show how OC MAR is calculated (Site U1337). A flow chart that uses data from Site 1337 as an example to illustrate the procedures of deriving the sedimentation rate (**b**) from the age-depth relationship (**a**), together with the TOC% and dry bulk density data (**c**) to produce the (**d**) TOC mass accumulation rate (MAR).

Extended Data Fig. 9 | Controlling factors for OC burial in our studied sites. a. map shows either TOC% or sedimentation rate (SR) control on OC burial rates of each site. **b.** A histogram to present the number and percentage of sites controlled by either TOC%, or SR, as well as the ones with unclear relationships.

Extended Data Table 1 | Information of the modified Longhurst biogeochemical provinces used in this study and their associated TOC MARs records.

Supplemental Data File 1 | Site information and TOC MARs.

Supplemental Data File 2 | Longhurst biogeochemical province information and their modern/Neogene OC burial.

Supplemental Data File 3 | IHO ocean zonation information and their modern/Neogene OC burial.

Supplemental Data File 4 | FAO ocean zonation information and their modern/Neogene OC burial.

Supplemental Data File 5 | IODP sites paleogeography and visualization of their TOC MARs over the Neogene.

Supplemental Data File 6 | Neogene global OC burial changes according to carbon cycle models.

Supplemental Data File 7 | Calculations of the flux and isotopic value of Neogene carbon input into the surficial system.

Supplemental Data File 8 | Linear fitting results between TOC MARs and SR, TOC%, and DBD of each site.

Supplemental Data File 9 | Sadler effect evaluation.

Supplemental Data File 10 | Location, water depth and distance of sites used in Extended Data Fig. 2.

Data Availability

All individual site, regional and global OC burial data, calculations for region and global OC burial rates and the Neogene global carbon cycle are available at Figshare (https://doi.org/10.6084/m9.figshare.21001849). These data are also archived as Supplementary Data Files (1-10) associated with the online version of this article.

Code Availability

The algorithm used to calculate regional and global OC burial from TOC MAR of individual sites is publicly available as MATLAB and R code package on GitHub (https://github.com/Ziyeli-moc/OC-burial.git).

Cited References

52. Zachos JC, Dickens GR, Zeebe RE. An early Cenozoic perspective on greenhouse warming and carbon-cycle dynamics. *Nature* 2008, **451:** 279-283.

53. Rae JWB, Zhang YG, Liu X, Foster GL, Stoll HM, Whiteford RDM. Atmospheric CO_2 over the past 66 million years from marine archives. *Annu Rev Earth Planet Sci* 2021, **49:** 609-641.

54. Dunne JP, Sarmiento JL, Gnanadesikan A. A synthesis of global particle export from the surface ocean and cycling through the ocean interior and on the seafloor. *Global Biogeochem Cycles* 2007, **21:** GB4006.

55. Molnar P, England P. Late Cenozoic uplift of mountain ranges and global cliamte change: Chicken or egg? *Nature* 1990, **346:** 29-34.

56. Lazarus DB. Neptune: A marine micropaleontology database. *Mathematical Geology* 1994, **26:** 817-832.

57. Spencer-Cervato C. The Cenozoic deep sea microfossil record: Explorations of the DSDP/ODP sample set using the Neptune database. *Palaeontologia electronica* 1999, **2:** 270.

58. Meyers PA, Silliman JE. Organic matter in Pleistocene to Quaternary turbidites from Sites 897, 898, 899 and 900, Iberia Abyssal Plain. In: Whitmarsch RB, Sawyers DS, Klaus A, Masson DG (eds). *Proceedings of the Ocean Drilling Program, Scientific Results*, vol. 149. Ocean Drilling Program: College Station, TX, 1996, pp 305-313.

59. Olivarez Lyle A, Lyle M. 20. Organic carbon and barium in Eocene sediments: Possible controls on nutrient recycling in the Eocene equatorial Pacific Ocean. In: Wilson PA, Lyle M, Firth JV (eds). *Proceedings of the Ocean Drilling Program, Scientific Results*, vol. 199. Ocean Drilling Program: College Station, TX, 2005, pp 1-33.

60. Shipboard Scienfitic Party. 12. Site 1219. In: Lyle M, Wilson PA, Janecek TR (eds). *Proceeding of the Ocean Drilling Program, Initial Reports*, vol. 199. Ocean Drilling Program: College Station, TX, 2002.

61. Expedition 306 Scientists. Site U1312-U1315 methods. In: Channell JET, Kanamatsu T, Sato T, Alvarez Zarikian CA, Malone MJ, the Expedition 303/306 Scientists (eds). *Proceedings of the Integrated Ocean Drilling Program*, vol. 303/306. IODP: College Station, TX, 2006.

62. Expedition 317 Scientists. Methods. In: Fulthorpe CS, Hoyanagi K, Blum P, the Expedition 317 Scientists (eds). *Proceedings of the Integrated Ocean Drilling Program*, vol. 317. IODP: College Station, TX, 2011.

63. Galy V, France-Lanord C, Beyssac O, Faure P, Kudrass H, Palhol F. Efficient organic carbon burial in the Bengal fan sustained by the Himalayan erosional system. *Nature* 2007, **450:** 407-410.

64. France-Lanord C, Derry LA. Organic carbon buria forcing of the carbon cycle from Himalayan erosion. *Nature* 1997, **390:** 65-67.

65. Sclater JG, Anderson RN, Bell ML. Elevation of ridges and evolution of the central eastern Pacific. *J Geophys Res* 1971, **76:** 7888-7915.

66. Burdige DJ. Preservation of organic matter in marine sediments: controls, mechanisms, and an imbalance in sediment organic carbon budgets? *Chemical Reviews* 2007, **107:** 467-485.

67. Hayes CT, Costa KM, Anderson RF, Calvo E, Chase Z, Demina LL*, et al.* Global Ocean sediment composition and burial flux in the deep sea. *Global Biogeochem Cyc* 2021, **35:** e2020GB006769.

68. Muller RD. GPlates: Building a virtual Earth though deep time. *Geochem Geophys Geosyst* 2018, **19:** 2243-2261.

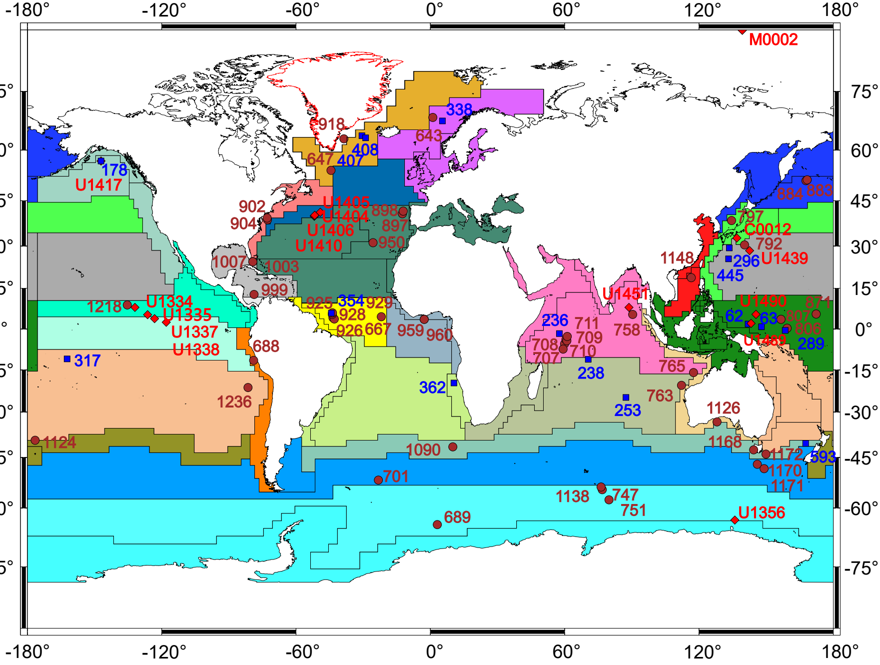
-180°
-120°
-60°
0°
60°
120°
180°
75°
60°
45°
30°
15°
0°
-15°
-30°
-45°
-60°
-75°
M0002
338
918
643
408
407
647
178
U1417
U1405
898
902
U1404
904
897
U1406
950
U1410
1007
1003
999
925
354
929
1218
U1334
928
U1335
926
667
959
960
U1337
U1338
688
317
1236
362
1124
1090
701
689
236
711
709
708
710
707
758
U1451
238
253
765
763
1126
1168
1172
1170
1171
593
1138
747
751
U1356
883
884
797
C0012
792
1148
296
U1439
445
U1490
871
62
63
807
806
U1489
289

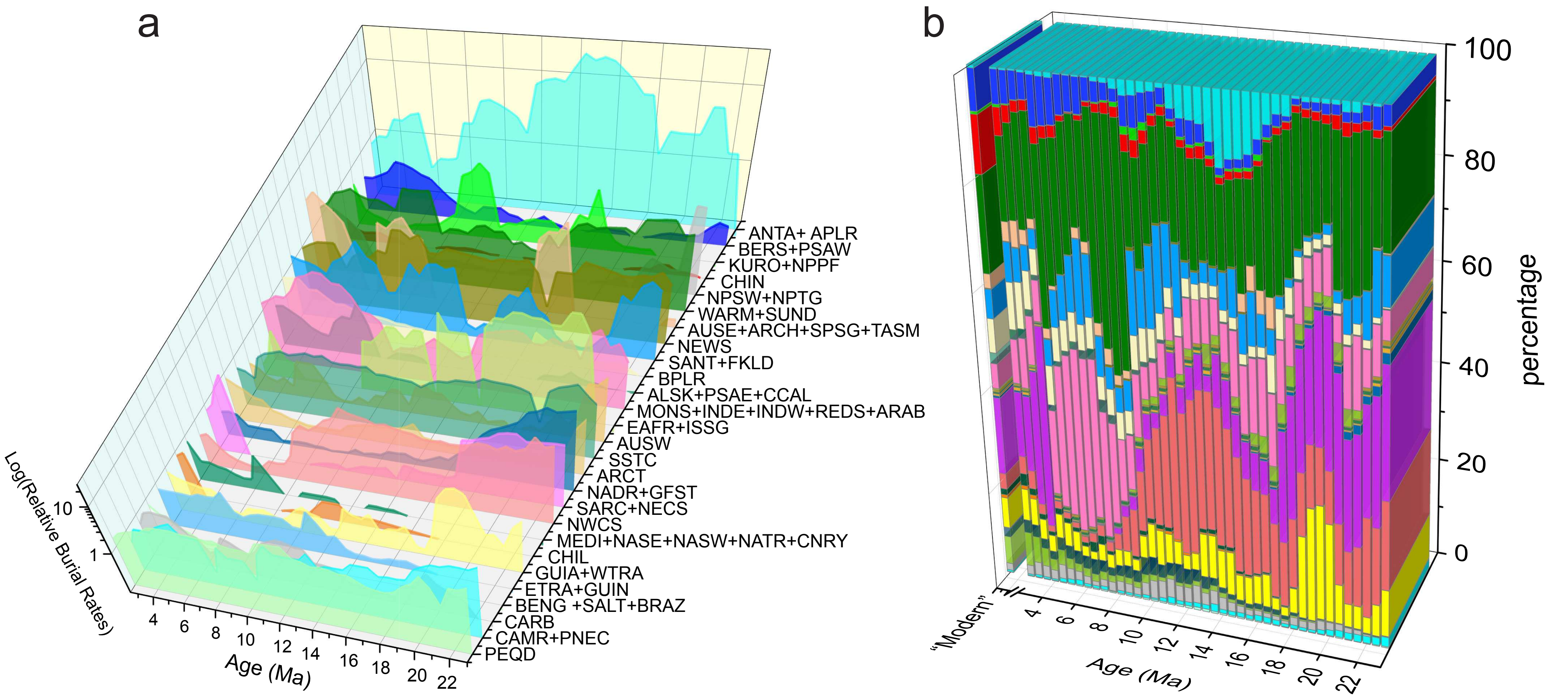
a
b
Log(Relative Burial Rates)
10
1
4
6
8
10
12
14
16
18
20
22
Age (Ma)
ANTA+ APLR
BERS+PSAW
KURO+NPPF
CHIN
NPSW+NPTG
WARM+SUND
AUSE+ARCH+SPSG+TASM
NEWS
SANT+FKLD
BPLR
ALSK+PSAE+CCAL
MONS+INDE+INDW+REDS+ARAB
EAFR+ISSG
AUSW
SSTC
ARCT
NADR+GFST
SARC+NECS
NWCS
MEDI+NASE+NASW+NATR+CNRY
CHIL
GUIA+WTRA
ETRA+GUIN
BENG +SALT+BRAZ
CARB
CAMR+PNEC
PEQD
100
80
60
40
20
0
percentage
"Modern"
Age (Ma)

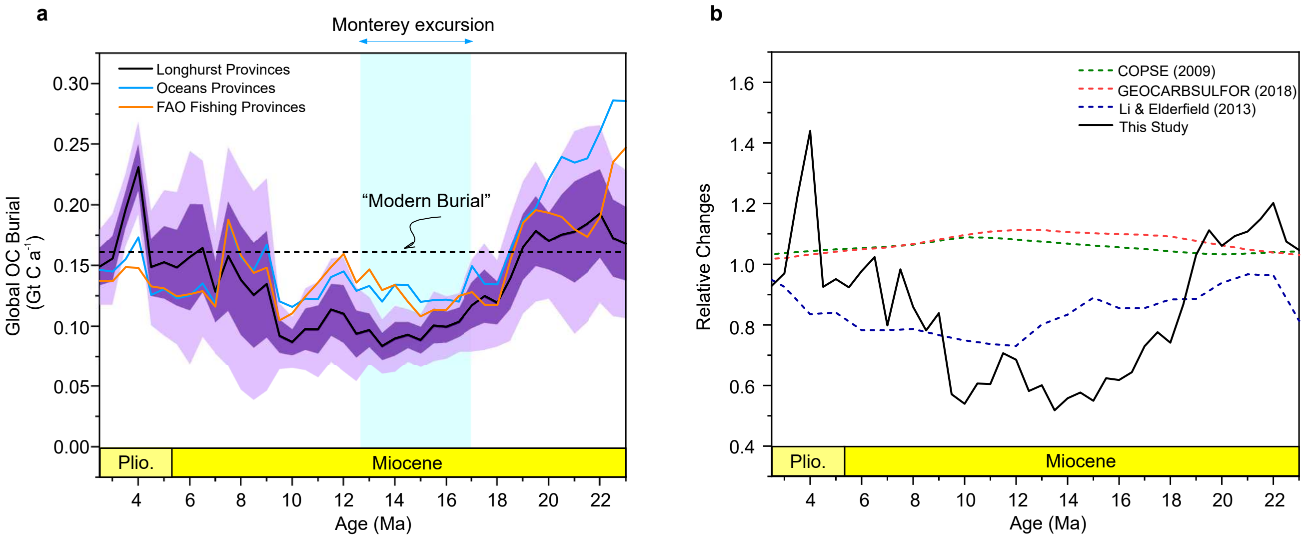
a
Monterey excursion
Longhurst Provinces
Oceans Provinces
FAO Fishing Provinces
"Modern Burial"
Global OC Burial
(Gt C a^{-1})
0.30
0.25
0.20
0.15
0.10
0.05
0.00
Plio.
Miocene
4
6
8
10
12
14
16
18
20
22
Age (Ma)
b
COPSE (2009)
GEOCARBSULFOR (2018)
Li & Elderfield (2013)
This Study
Relative Changes
1.6
1.4
1.2
1.0
0.8
0.6
0.4
Plio.
Miocene
4
6
8
10
12
14
16
18
20
22
Age (Ma)

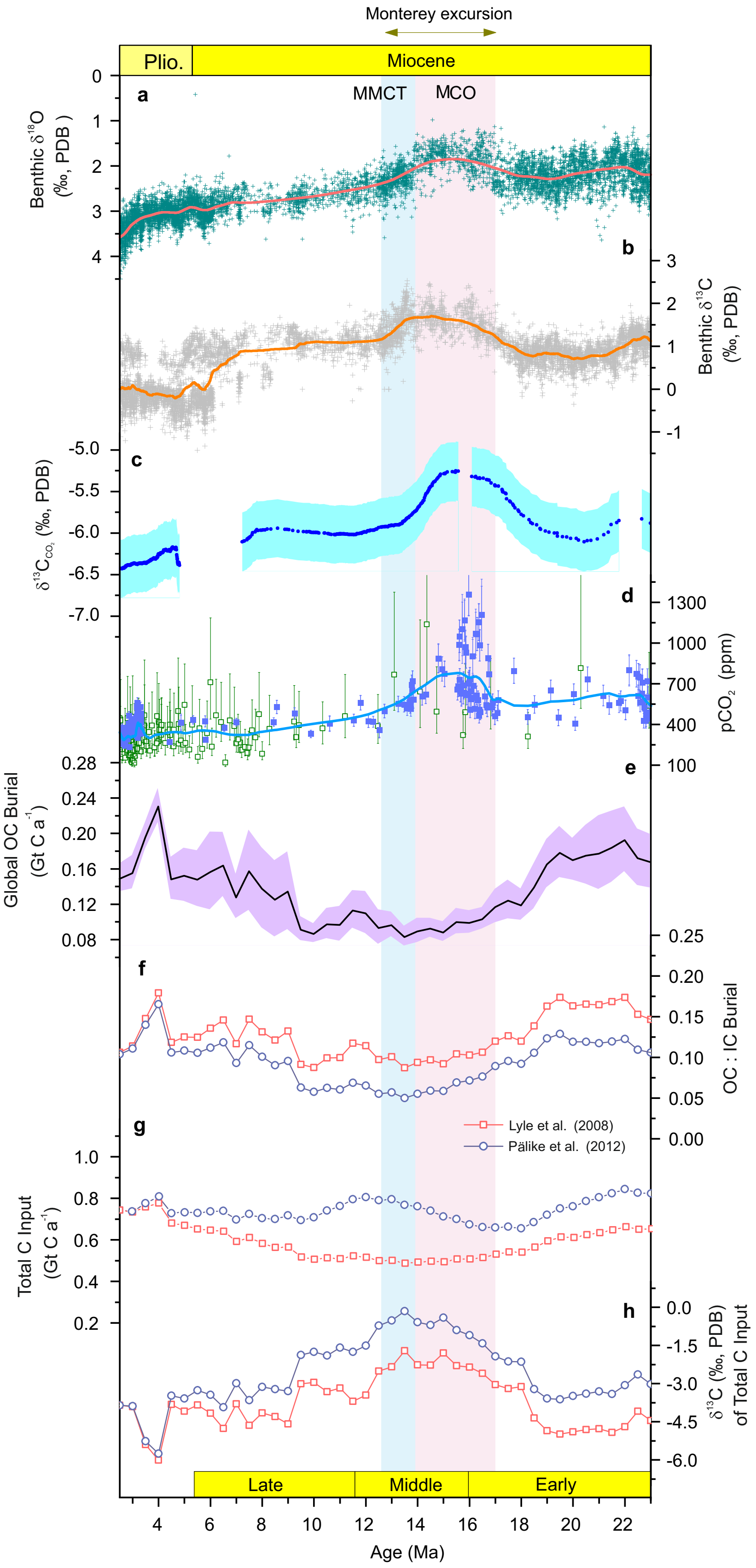

Monterey excursion
Plio.
Miocene
a
MMCT
MCO
Benthic $\delta^{18}O$ (‰, PDB)
b
Benthic $\delta^{13}C$ (‰, PDB)
c
$\delta^{13}C_{CO_2}$ (‰, PDB)
d
pCO_2 (ppm)
e
Global OC Burial (Gt C a^{-1})
f
OC : IC Burial
g
Lyle et al. (2008)
Pälike et al. (2012)
Total C Input (Gt C a^{-1})
h
$\delta^{13}C$ (‰, PDB) of Total C Input
Late
Middle
Early
Age (Ma)